



Team 19

Team Members:

Joseph Kavanagh
- 13040995

Brendan McKenna
- 13025360

Oscar Gordon-Christopher
- 13021757

Flight Test Coursework

UFMFCH-15-3 Spaceflight



Abstract

The project aim is to evaluate and model a microlight aeroplane, the aircraft under investigation is the EV-97 team EUROSTAR UK. The first part of this project involves the analysis of flight test data to ascertain its validity. This allows climb and descent performance to be obtained and the stability of the EV-97 in phugoid, Dutch and spiral modes. To be approximated.

Following on, a flight dynamic model is created using Simulink, a tool provided by the MATLAB software suite. Within this overall system there are numerous models, such as longitudinal and lateral, which are built from the equations of motion and their derivatives. This allows the virtual simulation, to model the different motions of flight and test the stability of the aircraft in all axes (X, Y, Z). It also allows for an increased accuracy and precision through continued iterations, and the ability for faster reruns.

This allows for a comparison to be generated between both methods and the differences between each to be identified. Variance was observed between approximations, actual flight data and Simulink models of natural frequency and damping ratio.

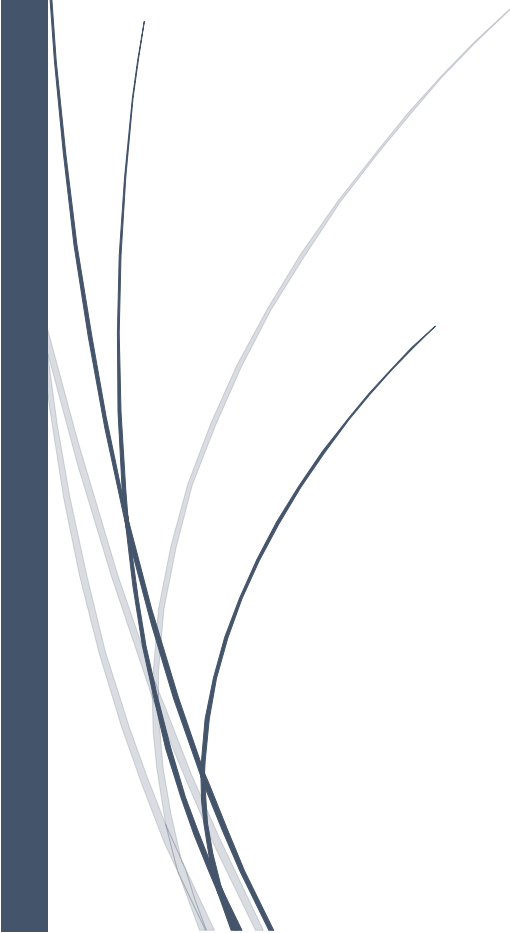


Table of Contents

Abstract	0
List of Tables	3
List of Figures	3
1.0 Team Members	4
2.0 Introductions	4
2.1 Aim	4
2.2 Aircraft	4
3.0 Weight and Balance Calculations	6
4.0 Actual Flight Data	7
4.1 Data Collection	7
4.2 Data Validation	7
4.3 Climb Performance	7
4.4 Descent Performance	8
4.5 Phugoid Approximations	8
4.6 Dutch Roll	10
4.7 Spiral Stability	11
4.8 Short Period	11
5.0 Computational Modelling	12
5.1 Introduction	12
5.1 Governing Equations of Flight Simulators	12
5.2 Euler Rotational Matrix	13
5.3 Phugoid Model	13
5.4 Configuration of Eurostar	11
5.5 Longitudinal Calculations	11
5.6 Lateral Model	13
5.6.1 Spiral Approximation	14
5.6.2 Roll Approximation	15
5.6.3 Short Period Approximation	15
5.6.4 Dutch Roll Approximation	15
5.6.5 Phugoid Approximations	15
6.0 Results and System Model	17
6.1 Flight Dynamic Model	17
6.2 Results	18
6.3.1 Phugoid, Short Period and Dutch Roll	18
6.2.2 Simulink Model	19

6.3 Improvements	12
6.3.1 Flight Data Improvements	12
6.3.2 Model Improvements	12
6.3.3 MERLIN Flight Simulator	12
7.0 Conclusion	13
8.0 References	14
9.0 Appendix	15
9.1 Flight Test Card A	15
9.2 Flight test Card B	16

List of Tables

Table 1 - Team and Contributions.....	4
Table 2 - Technical Data of EV-97	5
Table 3 - Phugoid Variable Data.....	9
Table 4 - Dutch Roll Results from Data	10
Table 5 - Initial Gravitational and Thrust Force Equations	12
Table 6 - Longitudinal Derivative Variable Equations	11
Table 7 - Values that can be obtained from the Resources	12
Table 8 - Derivative Table for Lateral Model	13
Table 9 - Damping Ratio and Natural Frequency Table	18

List of Figures

Figure 1 - EV-97 Microlight Aeroplane.....	4
Figure 2 - EV-97 Weight Balance Table	6
Figure 3 - Weight Balance Graph for EV-97	6
Figure 4 - Climb Performance of EV-97 from Actual Data	8
Figure 5 - Descent Performance of EV-97 from Actual Data	8
Figure 6 - Phugoid Approximation of EV-97 from Actual Data	9
Figure 7 - Dutch Roll ^[8]	10
Figure 8 - Initial Flight Dynamic Model for Cessna 172	12
Figure 9 - Axes about Fixed Wing Aircraft.....	12
Figure 10 - Euler Rotation Representation	13
Figure 11 - Longitudinal Sub-System Model	12
Figure 12 - Graphical Representation of Longitudinal Model.....	12
Figure 13 - Lateral Sub-System Model	13
Figure 14 - Graphical Representation of Lateral Model	14
Figure 15 - Spiral Divergence	15
Figure 16 - Flight Dynamic System.....	17
Figure 17 - Lateral Scope.....	19
Figure 18 - Longitudinal Scope.....	19
Figure 19 - Longitudinal Matrix Graph.....	20
Figure 20 -Lateral Matrix Graph.....	20
Figure 21 - End positon in 3D Visualisation	11
Figure 22 – Beginning of 3D Visualisation.....	11
Figure 23 - Test Card with observed Spiral Instability	12
Figure 24 - EXCALIBUR Flight Model Editor	12

1.0 Team Members

The team that worked on this project and report, with their relevant contribution, are detailed in table 1.

Table 1 - Team and Contributions

Name	Student Number	Contribution
Joseph Kavanagh	12040995	100%
Brendan Mckenna	13025360	100%
Oscar Gordon-Christopher	13021757	100%

2.0 Introductions

2.1 Aim

The aim of the project is compare both theoretical and actual flight data. It is also to analyse the static and dynamic stability of the aircraft under investigation. The comparison of these two sets of data will be achieved through the creation of a computer model generated using MATLAB and Simulink. Even though the project focuses on one particular aircraft model, the theory and method for analysis can be used on any aircraft.

During the actual test flights several characteristics were monitored, the first characteristics monitored were the aircrafts climb and descent performance. Following this the stability of the aircraft was monitored which included, phugoid motion, short period and Dutch roll. These will be then be compared and verified with the computational results.

Computational modelling of these characteristics is important when designing an aircraft, it allows prediction of the handling of the aircraft before flight testing. It also helps designers identify the role that the aircraft will have, through the stability. The aircraft under investigation can be predicted to be stable, due to its intended role, however for example military aircraft such as the F-16 and Eurofighter Typhoon are designed be to be unstable which increases the manoeuvrability. ^[1]

2.2 Aircraft

The aircraft under investigation is the EV-97 teamEUROSTAR UK microlight aeroplane, manufactured by Evektor-Aerotechnik, it is shown in figure 1. ^[2] It is intended for recreational and touring flying but limited to non-aerobatic operation in visual meteorological conditions (VMC). It is a single engine, two seater, all metal, low-wing monoplane with a semi-monocoque airframe structure. The two seats are side-by-side and the aircraft is installed with a fixed tricycle undercarriage and steerable nose wheel.

The aircraft is powered by a ROTAX 912 (80 hp) engine. It is a 4-stroke, 4 cylinder horizontally opposed, spark ignition engine with an electric starter, alternator and mechanical fuel pump. This engine drives a two blade, fixed pitched wooden propeller (V 230C). ^[2]

Table 2 contains some the technical data published in the pilot operating handbook (POH). ^[2]



Figure 1 - EV-97 Microlight Aeroplane

Table 2 - Technical Data of EV-97

Wing		
Span	8.1 m	26.57 ft
Area	9.84 m ²	105.92 ft ²
Mean Aerodynamic Centre (MAC)	1.25 m	4.10 ft
Wing Loading	45.7 kgm ⁻²	9.37 lbft ⁻²
Aileron Area	0.21 m ²	2.26 ft ²
Flap Area	0.52 m ²	5.60 ft ²
Fuselage		
Length	5.98 m	19.62 ft
Width	1.04 m	3.41 ft
Height	2.34 m	7.67 ft
General Characteristics		
Manoeuvring Speed (V_A)	44.70 ms ⁻²	100mph
Max. Structural Cruise Speed (V_{NO})	52.75 ms ⁻²	118 mph
Max. Take-off Weight	450 kg	992 lbs
Empty Weight	268 kg	591 lbs
Max. Fuel	65 litres	14.3 gals
Service Ceiling	50292 m	16500 ft

3.0 Weight and Balance Calculations

Before any flight, the longitudinal static stability of the aircraft needed to be identified, this is so that any added weight and its position does not negatively affect the manoeuvrability and control. Within the POH, a table and graph displaying a weight against balance is shown, this allows the pilot to identify the centre of gravity (C.G.) and whether it is within the safe bounds of operation. Figure 2 shows the weight balance table from the EV-97 POH. [2]

Maximum Permitted Crew Weight for given Baggage and Fuel Loads, kg.								
Date	Empty weight kg	Empty C.G. posn. mm AOD	FUEL LOAD				Approved	
			Fuel gauge	1	3/4	1/2	1/4	
			Fuel volume	62 litres	47 litres	31 litres	15 litres	Date
			Fuel weight	45 kg	33 kg	22 kg	11 kg	Signature
			max. 15kg					
			1/2 = 8 kg					
			None					
			max. 15kg					
			1/2 = 8 kg					
			None					
			max. 15kg					
			1/2 = 8 kg					
			None					
			max. 15kg					
			1/2 = 8 kg					
			None					
			max. 15kg					
			1/2 = 8 kg					
			None					

Figure 2 - EV-97 Weight Balance Table

However to increase accuracy of this model, MATLAB was used to create a weight balance graph for the EV-97, this allows for increased accuracy and faster repeats. The model also allows for user inputs, such as crew, baggage/payload and fuel weights. To create this graph the POH was used extensively to obtain numerous values relating to the aircraft variables. Equation (3.0) identifies the principal equation that was used to create the weight balance graph within MATLAB.

$$x_{cg} = \frac{\text{Total Moment}}{\text{Total Weight}} \quad (3.0)$$

Figure 3 is the weight balance graph obtained from MATLAB, the red X shows when there is a payload of 10kg, crew weight of 60kg and filled up with 10 litres of fuel. The box that is observed on graph, is the operational safety limits for the aircraft, if the cross is outside this limit then there will be a noticeable decrease in static stability. The model can be operated on a continuous loop so that the aircraft C.G. is always known, even as the fuel weight decreases as it is used up. This is especially important in large commercial and military aircraft where the larger quantities of fuel and mission payloads are present, and decreases in total weight are more noticeable. A continuous looped model will allow for the pilot to account for this change in C.G. or for a fuel management system to move the fuel around like in the A380.

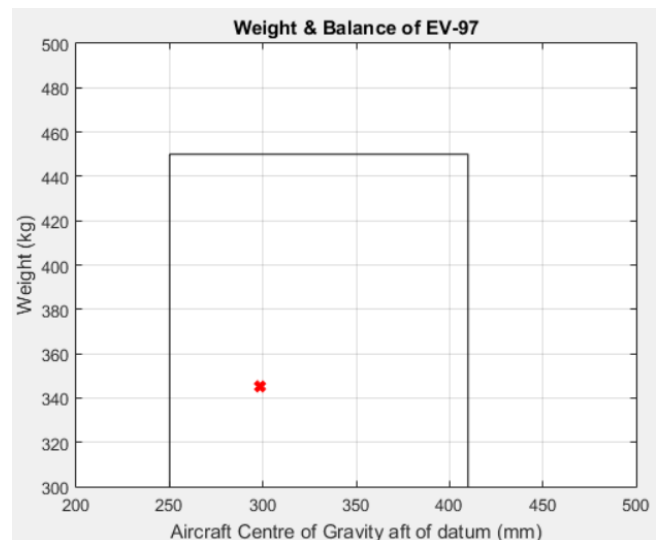


Figure 3 - Weight Balance Graph for EV-97

4.0 Actual Flight Data

4.1 Data Collection

The data that was collected and recorded from the cockpit of the EV-97 over the course of an hour flight. This data was collected the previous year by level 3 aerospace engineering students. The test cards collected information on numerous variables, which can be found below:

- Atmospheric Condition (Pressure and Temperature)
- Crew Information (Weight)
- Fuel Weight (Take-off/Landing)
- Timing Information (Tacho start to finish)
- Climb and Descent Performance
- Phugoid Characteristics
- Roll and Spiral Mode Characteristics

The numerical data obtained can be used to calculate the aerodynamic characteristics of the aircraft, however some of the recorded sections were only observational comments about the performance of the aircraft. As well as the flight data, the aircraft's weight and balancing were also recorded to account for the passenger's weight and also the loss of fuel as the flight progressed. Any anomalous results could have been a consequence of human or instrumentation errors.

The test cards used for data collection are found in the appendix (section 9.1 and 9.2).

4.2 Data Validation

This data set was analysed for any anomalous, incomplete or absent readings by comparing every data set. Those test cards that were missing data were ignored so that they did not affect the overall results, however there was still plenty of data to begin and complete analysis of the aircraft.

Also as the data was taken over a period of time, the weather conditions changed from flight to flight and day to day. So as to compensate for this, all data collected on every flight was used in the model to create an average and provide an even characteristic of the performance for the aircraft.

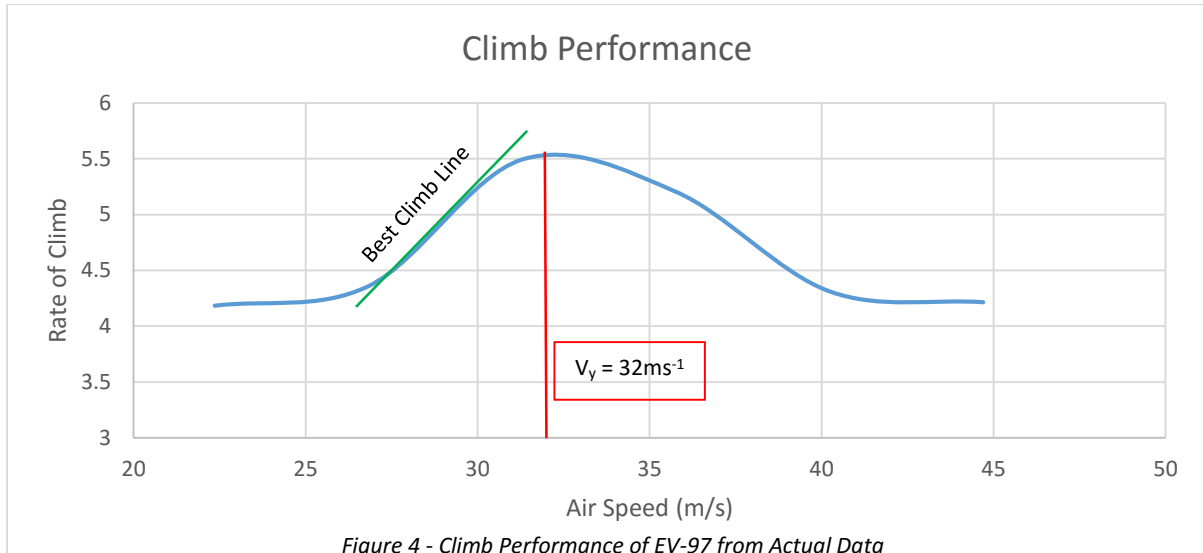
4.3 Climb Performance

After the data was checked for anomalous results, climb performance of the aircraft can be calculated. First the required data was converted to SI units before being used to calculate the rate of climb (ROC), equation (4.0). The data from the test cards, contained the starting altitude and fuel, the finishing altitude and fuel, as well as the crew weight, speed of climb and time taken of climb.

The climb performance is calculated using equation (4.1) and the result is shown in figure 4. The maximum rate of climb is identified on figure 4 when the airspeed is 32ms^{-1} (72mph), this value is confirmed in the POH, indicating that the aircraft still operates to the manufacturer's specification.

$$ROC \text{ or } ROD = \frac{\text{change in altitude (m)}}{\text{time taken (t)}} \quad (4.0) \qquad ROC_{MAUW} = ROW_{test} \left(\frac{W_{test}}{W_{MAX}} \right) \quad (4.1)$$

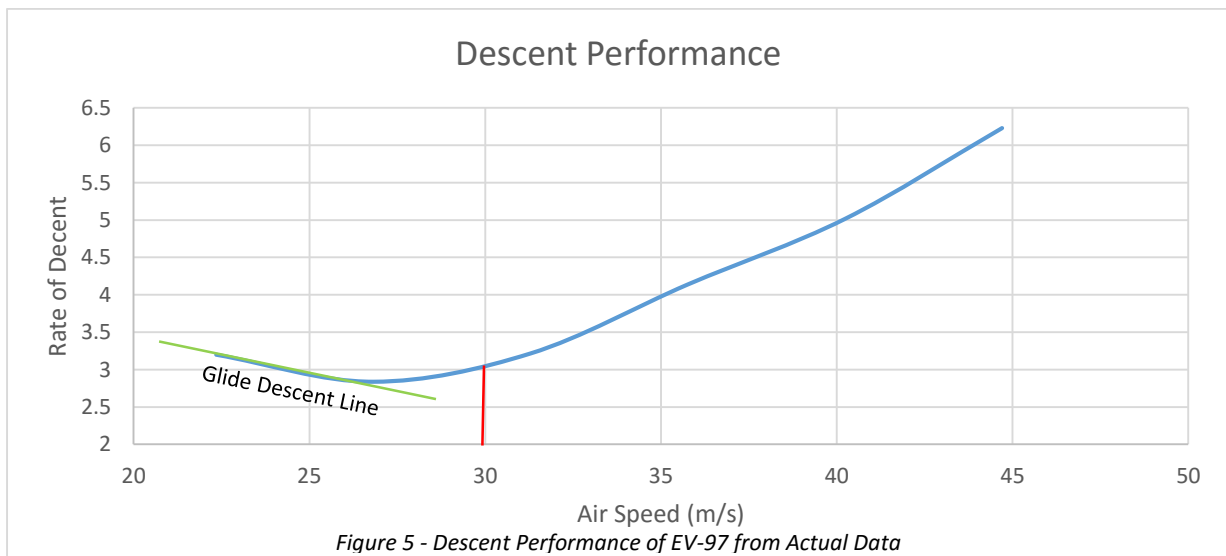
The curve in figure 4 shows the climb rate with relation to the air speed of the aircraft at maximum all-up weight. The best climb rate (V_y) is at 32ms^{-1} and the best climb line can also be seen on the graph.



4.4 Descent Performance

The descent phase is the opposite to the climb phase of flight, but it still needs to have a consistent performance to provide stable flight. The POH states the descent velocity to be at 30 ms^{-1} (68mph). Using equation (4.2) to obtain the maximum all-up weight rate of descent (ROD_{MAUW}), which leads to figure 5.

$$ROD_{MAUW} = ROD_{test} \sqrt{\frac{W_{MAUW}}{W_{test}}} \quad (4.2)$$



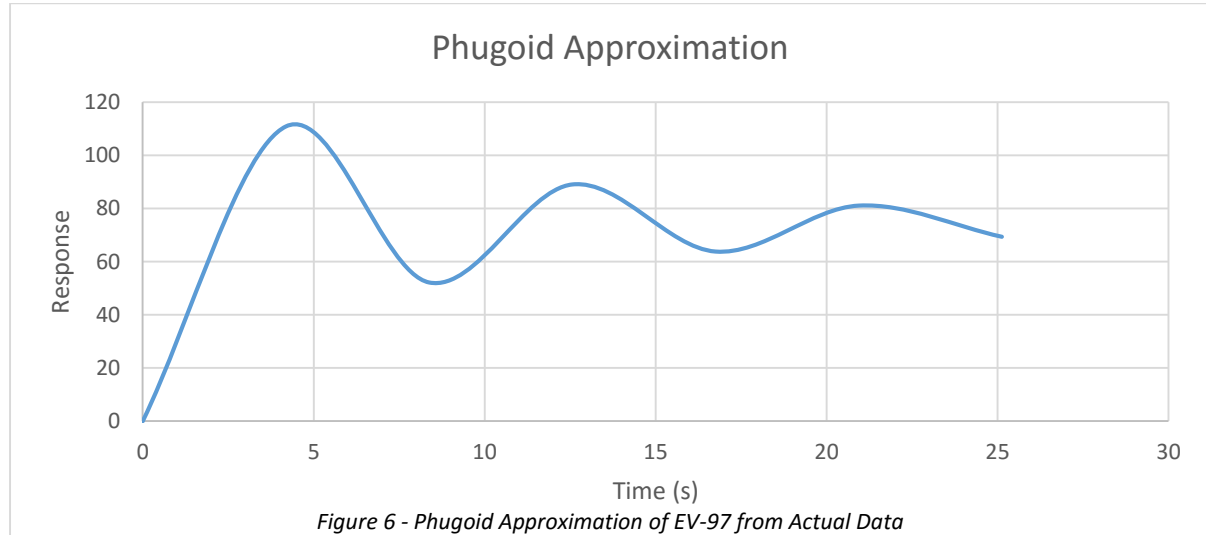
The optimal unpowered glide for descent can be seen on figure 5, and also the descent velocity found from the data show it to be similar to what is stated in the POH, indicating the aircraft is operating at manufactures specification. An increase in the rate of descent will lead to an increase in airspeed but a decrease in manoeuvrability and control.

4.5 Phugoid Approximations

Phugoid mode is essentially a slow sinusoidal movement where the height and forward speed vary whilst the angle of incidence remains constant. The effects of inertia and damping forces are very low as the motion of the oscillation is so slow. It can be taken that the phugoid oscillation is effectively a

fluctuation of potential and kinetic energy about a datum, where the aircraft is trying to stabilise. The pilot is easily able to control this motion because the period of oscillation is so large. ^[5]

From the test card data it is possible to display the phugoid motion that the aircraft responds to when disturbed. This is shown in figure 6, and the aircraft can be predicted to have a damped oscillation.



Further analysis of this data allows for the damping ratio (ζ), natural frequency (ω_n), damped natural frequency (ω_d) and settling time ($t_s(95\%)$) to be calculated, using the following equations: ^[6]

$$\delta = -\ln \frac{|r_3 - r_1|}{|r_2 - r_1|} \quad (4.3)$$

$$\zeta = \frac{\delta}{\sqrt{\pi^2 + \delta^2}} \quad (4.4)$$

$$\omega_d = \frac{2\pi}{t_3 - t_1} \quad (4.5)$$

$$\omega_n = \frac{\omega_d}{\sqrt{1 - \zeta^2}} \quad (4.6)$$

$$t_s(95\%) = \frac{3}{\zeta \omega_n} \quad (4.7)$$

Table 3 shows the resultant values obtained from the previous equations, the damping ratio is $\zeta < 1$ which confirms that it has a damped oscillation. It has quite a low damping ratio but that is to be expected, as an aircraft with a lower settling time will lead to an increased stress on the aircraft structure, possibly leading to damage and failure.

Table 3 - Phugoid Variable Data

Variable	Data
r1	110.92
r2	52.20
r3	89.08
r4	63.84
r5	81.12
r6	69.40
ζ	0.300291
ω_d	0.750297 Hz
ω_n	0.7866 Hz
$t_s(95\%)$	12.70 seconds

From here this allows stability derivatives to be calculated, using the second order response characteristic equation (4.8), and leading onto equation (4.9) to solve the system of eigenvalues. ^[7]

$$\frac{R(s)}{C(s)} = \frac{\omega_n^2}{s^2 + 2\zeta\omega_n s + \omega_n^2} \quad (4.8)$$

$$\lambda^2 - X_u - g \frac{Z_u}{u_0} = \lambda^2 + 2\zeta\omega_n\lambda + \omega_n^2 \quad (4.9)$$

This leads to $X_u = -0.47242$ and $Z_u = \sqrt{\frac{-0.61874u_0}{9.81}}$.

4.6 Dutch Roll

Lateral stability is the roll stability. If the aircraft comes under a disruption from wind or other atmospheric conditions, the plane can roll. A dihedral angle on the wing will help rectify this and increase stability, as the lower wing will have a greater planform area than the upper wing, therefore creating greater lift and correcting the roll error e.g. the plane will roll but not turn. ^[7]

A sweepback on the wing allows the lower wing to catch up with the forward wing as it is more perpendicular to the flow of air, meaning the lift is greater and the drag is less, correcting the directional and roll instabilities. Vertical stability is produced by the force of wind on the vertical stabiliser.

If the vertical and lateral stability are working, but are out of phase with one another, oscillations will occur in the roll and yaw planes, this is known as Dutch roll. Transport aircraft often need active yaw dampers to subdue this effect, figure 7 show the motion of Dutch Roll.

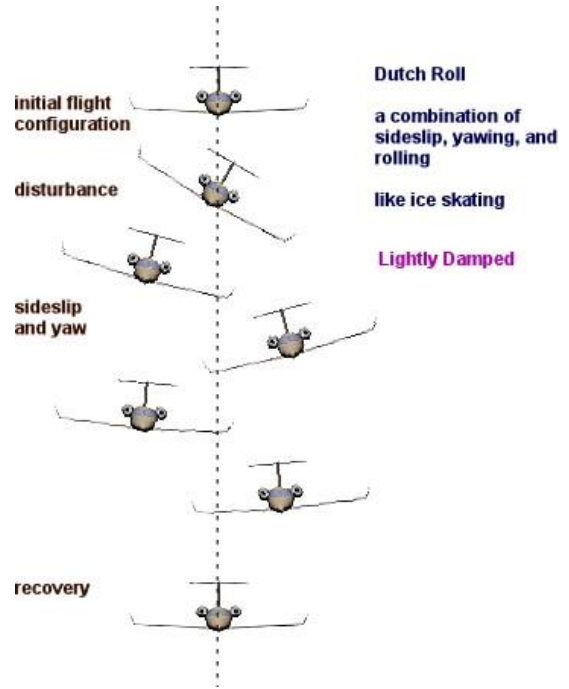


Figure 7 - Dutch Roll ^[8]

The following equations approximates the characteristics of Dutch Roll Mode ^[9] with the results show in table 4, from these results it can be said that the aircraft is quite stable and recovers.

$$\zeta_{DR} = \sqrt{\frac{1}{1 + \left(\frac{\eta}{\xi}\right)^2}} \quad (4.10)$$

$$\omega_{nDR} = \frac{-\xi_{DR}}{\zeta_{DR}} \quad (4.11)$$

$$T_{DR} = \frac{2\pi}{\omega_{nDR}\sqrt{1-\zeta_{DR}^2}} \quad (4.12)$$

$$N_{1/2DR} = \frac{\ln 2}{2\pi} \sqrt{\frac{1-\zeta_{DR}^2}{\zeta_{DR}}} \quad (4.13)$$

Table 4 - Dutch Roll Results from Data

Variable	Data
η	0.500224
ξ	0.395349
ζ_{DR} (Damping Ratio of Dutch Roll)	0.743294
ω_{nDR} (Undamped Natural F. Dutch Roll)	1.345362 sec ⁻¹
T_{DR} (Period Dutch Roll)	6.981317 sec
$N_{1/2DR}$ (Number of Cycles to half amplitude)	0.099286

4.7 Spiral Stability

If there is a weak dihedral angle when compared to a strong static stability, in effect on the aircraft then it will have a tendency to bank further and further. If left with no other input, it will eventually spiral into the ground, this is spiral instability. ^[7]

From the test cards it was identified that as the EV-97 rolls to the left to model spiral mode, the aircraft will diverge in the bank with a negative stability. However this is not observed when the aircraft rolls to the right and instead it will return to the neutral position, this means it is positively or neutral stable on the right side.

4.8 Short Period

A short period occurs when the aircraft is given a sudden stimulus. The incidence of the aircraft changes and so it will begin to pitch. For a stable aircraft such as the EV-97, the incidence will soon return to the original state because the damping is very high for this mode when compared to phugoid motion. The short period is also calculated using equations (4.10), (4.11) and (4.12).

From the test cards no numerical data was recorded, however many test cards noted that there was no oscillations observed and that the aircraft was over damped ($\zeta > 1$), which is to be expected of this type of aircraft.

5.0 Computational Modelling

5.1 Introduction

Throughout this section, MATLAB and Simulink are used to model the flight dynamics of the EV-97. The advantages of Simulink are immediately apparent as it is a graphical programming environment, this allows the system to be modelled using configurable block from numerous libraries. The blocks can then be specially scripted using MATLAB for the particular problem undertaken. Alongside this Simulink allows for Scope blocks to be embedded into the model wherever, the advantage of this is that it allows the user to monitor the responses anywhere in the system.

The performance and stability of the EV-97 will be obtained from test flight data and integrated with relevant theory to create an optimised flight dynamic model. Figure 8 shows the initial Simulink flight dynamic model. This model however is only simulates the longitudinal motion of a Cessna 172, and will need to be configured for the Eurostar EV-97 and lateral model completed.

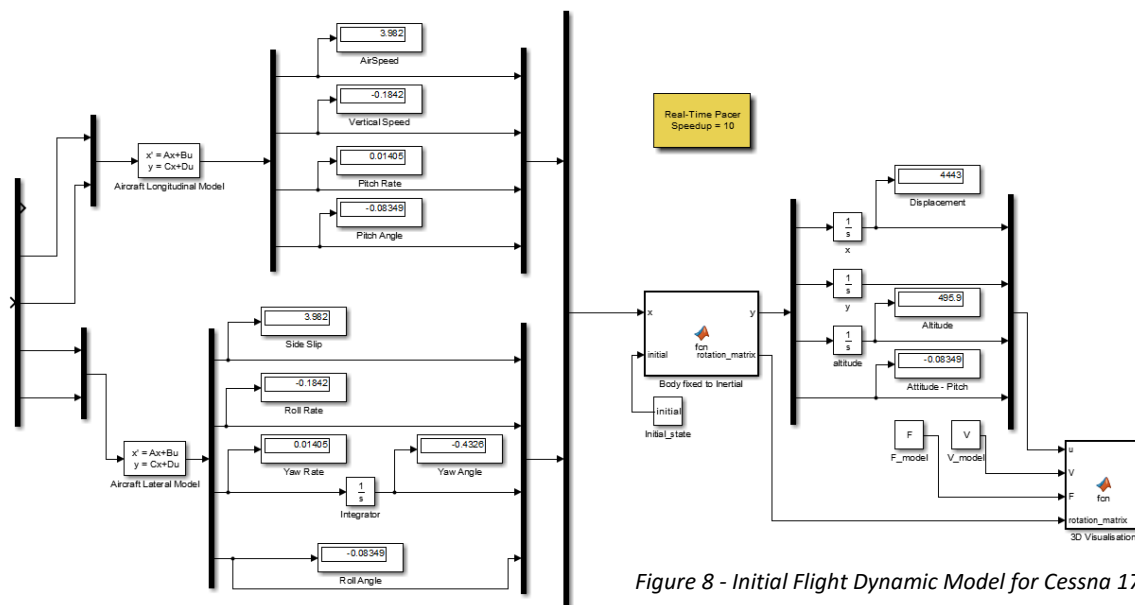


Figure 8 - Initial Flight Dynamic Model for Cessna 172

5.1 Governing Equations of Flight Simulators

Firstly the gravitational and thrust forces that act upon the aircraft different axes need to be defined. The axis of the aircraft are X, Y, Z and relate to Roll, Pitch and Yaw respectively, a diagrammatical model is presented in figure 9. [4] These initial equations to identify the forces are found in table 5.

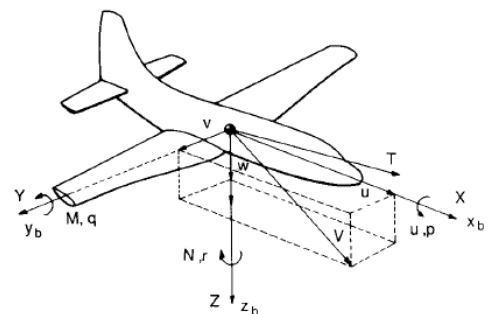


Figure 9 - Axes about Fixed Wing Aircraft

Table 5 - Initial Gravitational and Thrust Force Equations

Symbol	Definition	Equation
X_T	Net force on aircraft in X axis (e.g. Thrust – Drag)	$X = X_T - mg \sin \theta$
Y_T	Net force on aircraft in Y axis (e.g. Sideslip force during transition into bank)	$Y = Y_T + mg \cos \theta \sin \phi$
Z_T	Net force on aircraft in Z axis (e.g. lift)	$Z = Z_T + mg \cos \theta \sin \phi$

Following on from this, the non-linear rigid body equations of motion can be presented in equations (5.0), (5.1), (5.2), (5.3), (5.4) and (5.5), these are the underlying equation of flight simulations. The

subscript x, y, z, relates to the axis. The equations that relate to the longitudinal are (5.0), (5.2) and (5.4) where (5.1), (5.3) and (5.4) are related to the lateral model.

$$X_T - mg \sin \theta = m(\dot{u} + qw - rv) \quad (5.0)$$

$$L_T = \dot{H}_x + qH_z - rH_y \quad (5.3)$$

$$Y_T + mg \cos \theta \sin \phi = m(\dot{v} + ru - pw) \quad (5.1)$$

$$M_T = \dot{H}_y + rH_x - pH_z \quad (5.4)$$

$$Z_T + mg \cos \theta \cos \phi = m(\dot{w} + pv - qu) \quad (5.2)$$

$$N_T = \dot{H}_z + pH_y - qH_x \quad (5.5)$$

However these equations will need to be linearized to incorporate real world data and be able for better comparison of results.

5.2 Euler Rotational Matrix

Euler angles are used to describe the orientation of a rigid body, it was the first series of equations to be completed within the system model. The Euler rotational matrix is the last block in the system before 3D visualisation, all data from both longitudinal and lateral models pass through this matrix, with the output of this matrix being Euler angles. It relates data to and the forces to the relevant plane, for the 3D model. Figure 10^[10] shows the Euler angles, where the original system is shown in blue and the rotated system is shown in red.

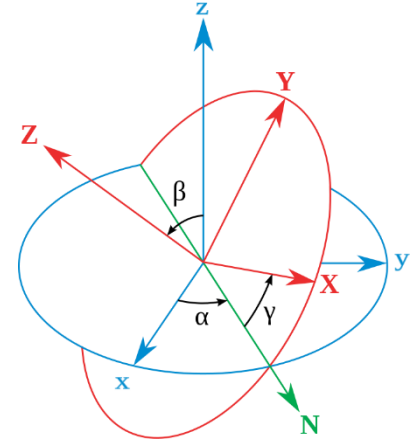


Figure 10 - Euler Rotation Representation

The Euler Rotational Matrix can be seen in equation (5.6)^[11], and will be recreated in a MATLAB script for the Euler block in the system model.

$$\begin{bmatrix} v_{x1} \\ v_{y1} \\ v_{z1} \end{bmatrix} = \begin{bmatrix} \cos \theta \cos \psi & \sin \phi \sin \theta \cos \psi - \cos \phi \sin \psi & \sin \phi \sin \psi + \cos \phi \sin \theta \cos \psi \\ \cos \theta \sin \psi & \cos \phi \cos \psi + \sin \phi \sin \theta \sin \psi & \cos \phi \sin \theta \sin \psi - \sin \phi \cos \psi \\ -\sin \theta & \sin \phi \cos \theta & \cos \phi \cos \theta \end{bmatrix} \begin{bmatrix} u \\ v \\ w \end{bmatrix} \quad (5.6)$$

5.3 Phugoid Model

The phugoid motion of the aircraft was modelled using a MATLAB script with a 'for' loop. All the test card data was put into an excel spreadsheet, allowing these values to be taken by MATLAB for further calculations. All the phugoid data was then run through equations (4.3), (4.4), (4.5) and (4.6), where then it was processed by statistical analysis with removal of anomalous results due to a refinement.

From the remaining values an average was taken, to obtain a more precise value for the coefficient of lift (C_l) and drag (C_d), at zero angle of attack (AoA). These coefficients are obtained by finding the stability derivatives X_u and Z_u , so that these values can be used in the configuration section, 5.4.

Equation (5.7) is initially used, where u_0 is a variable depending on the specific test card. Then C_{Zu} was calculated using (5.8), where m is the mass of the aircraft, S the planform area of the wing and Q is dynamic pressure related to the altitude. This allows C_{L0} to be found used (5.9). Similarly equations (5.10), (5.11) and (5.12) are then used to obtain an approximation of C_{D0} from the flight data.^[4]

$$Z_u = -\frac{\omega_n^2 u_0}{g} \quad (5.7)$$

$$C_{Zu} = \frac{mu_0 Z_u}{QS} \quad (5.8)$$

$$C_{L_0} = -\frac{C_{Zu}}{2} \quad (5.9)$$

$$X_u = -2\zeta\omega_n \quad (5.10)$$

$$C_{Xu} = \frac{mu_0 X_u}{QS} \quad (5.11)$$

$$C_{D_0} = -\frac{C_{Xu}}{3} \quad (5.12)$$

5.4 Configuration of Eurostar

The configuration of the Eurostar is the next phase of the system to be defined, this is one of the most important parts of this project, as both the longitudinal and lateral models will take values from this configuration. Also configuration files of other aircraft could be used in overall system as long as the configuration is compiled in the exact same way, with the variables defined the same as well.

Using the different resources, such as the POH, Javafoil, and the phugoid script, it is possible to obtain the flight characteristics and have a MATLAB script with all these values specified within it. This then allows the data to be called upon by both models, to calculate other variables. The main data that is defined in the configuration, regards the EV-97 measurements and aerodynamic properties. The measurements include the mean aerodynamic chord, wing span (b), wing area, length of aircraft, moment arms and tail area (S_t). The configuration will also call upon the coefficients obtained in phugoid model, so that they can be used in the longitudinal and lateral models.

5.5 Longitudinal Calculations

The aircrafts non-linear equations are found in section 5.1, however these are difficult to be incorporated into real world data and need to be linearised. With the longitudinal linearised equation of motion it becomes possible to compare and integrate the real world data. For the equation however small perturbation theory is assumed. This is a series of simplifications, assumptions and can be related to equation (5.13): ^[12]

$$v_0 = w_0 = p_0 = q_0 = r_0 = \phi_0 = \omega_0 = 0 \quad (5.13)$$

- Products of disturbance are negligible
- Reference flight condition are symmetric ★
- Propulsive forces are constant ★
- X-axis aligned with aircrafts velocity vector (\therefore no side slip) ★

The longitudinal linearised equations of motion (5.14) ^[13] are written in state space form. They are made up of two main matrices, the A matrix relates to the airframe model while the B matrix is the control inputs.

$$\begin{bmatrix} \Delta \dot{u} \\ \Delta \dot{w} \\ \Delta \dot{q} \\ \Delta \dot{\theta} \end{bmatrix} = \underbrace{\begin{bmatrix} X_u & X_w & 0 & -g \\ Z_u & Z_w & u_0 & 0 \\ M_u + M_{\dot{w}}Z_u & M_w + M_{\dot{w}}Z_w & M_q + M_{\dot{w}}u_0 & 0 \\ 0 & 0 & 1 & 0 \end{bmatrix}}_{\text{A matrix}} \begin{bmatrix} \Delta u \\ \Delta w \\ \Delta q \\ \Delta \theta \end{bmatrix} + \underbrace{\begin{bmatrix} X_{\delta e} & X_{\delta T} \\ Z_{\delta e} & Z_{\delta T} \\ M_{\delta e} + M_{\dot{w}}Z_{\delta e} & M_{\delta T} + M_{\dot{w}}Z_{\delta T} \\ 0 & 0 \end{bmatrix}}_{\text{B matrix}} \begin{bmatrix} \delta_e \\ \delta_T \end{bmatrix} \quad (5.14)$$

To define the variables in equation (5.14), the numerous equations in table 6 can be used. Table 7 states where some of the variables can be found that are used in the equations that are in table 6. ^[4]

Table 6 - Longitudinal Derivative Variable Equations

$X_u = \frac{-(C_{D_u} + 2C_{D_0})QS}{mu_0}$	$Z_u = \frac{-(C_{L_u} + 2C_{L_0})QS}{mu_0}$	$X_w = \frac{-(C_{D_\alpha} + 2C_{L_0})QS}{mu_0}$
$Z_w = \frac{-(C_{L_\alpha} + 2C_{D_0})QS}{mu_0}$	$M_{\dot{w}} = C_{m_\alpha} \left(\frac{\bar{c}}{2u_0} \right) \left(\frac{QS\bar{c}}{u_0 I_y} \right)$	$M_q = C_{m_q} \left(\frac{\bar{c}}{2u_0} \right) \left(\frac{QS\bar{c}}{I_y} \right)$
$M_u = C_{m_u} \frac{(QS\bar{c})}{u_0 I_y}$	$M_w = C_{m_\alpha} \frac{(QS\bar{c})}{u_0 I_y}$	$M_{\delta e} = C_{M_{\delta e}} \frac{(QS\bar{c})}{I_y}$
$M_{\delta e} = \frac{C_{Z_{\delta e}} QS}{m}$	$X_{\delta e} = 0$	-

Table 7 - Values that can be obtained from the Resources

From Flight Test Data		From POH	
Symbol	Definition	Symbol	Definition
C_{D_0}	Coefficient of Drag at 0 AoA	S	Wing Area
C_{L_0}	Coefficient of Lift at 0 AoA	\bar{c}	Mean aerodynamic chord length
u_0	Aircraft reference speed	m	Aircraft mass
Q	Dynamic Pressure		-

The longitudinal model is then created in MATLAB using the theory presented and related to relevant block in the Simulink model. This model simulates the pitch movement across the y-axis of the aircraft. The longitudinal model is present below in figure 11, the block surrounded by the red box is where the longitudinal matrix is located, while the second section of this sub-system just shows the different variables that are being produced as time progresses.

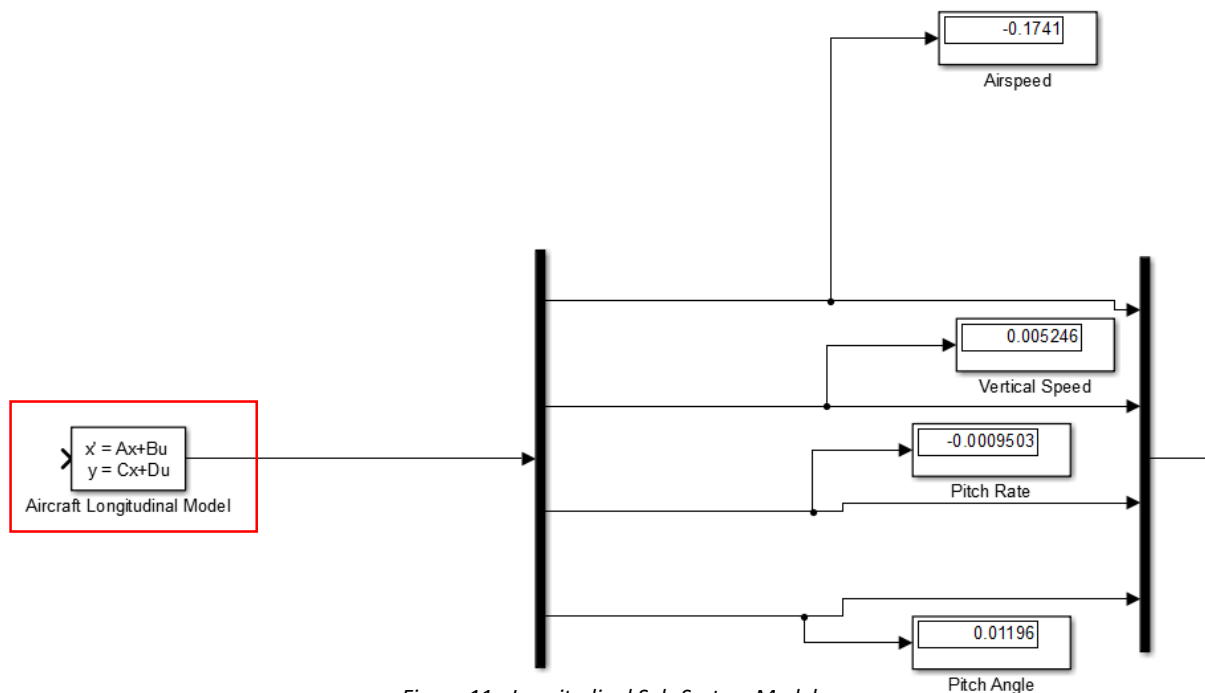


Figure 11 - Longitudinal Sub-System Model

When the model is run, a graphical representation of the motion of the aircraft is also generated. This is shown in figure 12 and allows a reference to whether the model is working as expected. At this point in the project the model showed a damped phugoid response and returned to straight and level flight.

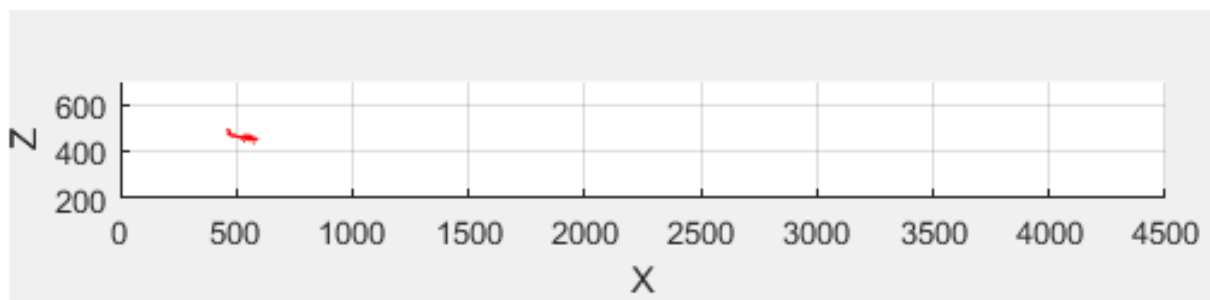


Figure 12 - Graphical Representation of Longitudinal Model

5.6 Lateral Model

This model is considered to be more complicated when compared to the longitudinal model. This is because when an airplane is disturbed from its equilibrium state it is a combination of rolling, yawing and sideslipping motions, increasing the complexity. The interacting between both roll and yaw creates a coupled motion, which needed to be understood and modelled to target potential lateral dynamic instabilities.

The lateral equation of motion for the Simulink is shown below, equation (5.14), it is presented in state space form. The A matrix relates to the aircraft model, while the B matrix control inputs. As before the variables for this equation are defined in table 8. ^[4]

$$\begin{bmatrix} \Delta \dot{v} \\ \Delta \dot{p} \\ \Delta \dot{r} \\ \Delta \dot{\phi} \end{bmatrix} = \begin{bmatrix} Y_v & Y_p & -(u_0 - Y_r) & g \cos \theta_0 \\ L_v & L_p & L_r & 0 \\ N_v & N_p & N_r & 0 \\ 0 & 1 & 0 & 0 \end{bmatrix} \begin{bmatrix} \Delta v \\ \Delta p \\ \Delta r \\ \Delta \phi \end{bmatrix} + \begin{bmatrix} 0 & \frac{Y_{\delta r}}{u_0} \\ L_{\delta a} & L_{\delta r} \\ N_{\delta a} & N_{\delta r} \\ 0 & 0 \end{bmatrix} \begin{bmatrix} \delta_a \\ \delta_r \end{bmatrix} \quad (5.14)$$

Table 8 - Derivative Table for Lateral Model

$Y_{\beta} = u_0 Y_v = \frac{C_{y\beta} QS}{m}$	$Y_p = \frac{C_{yp} Q S b}{2 m u_0}$	$Y_r = \frac{C_{yr} Q S b}{2 m u_0}$
$L_{\beta} = u_0 L_v = \frac{C_{l\beta} Q S b}{I_x}$	$L_p = \frac{C_{lp} Q S b^2}{2 I_x u_0}$	$L_r = \frac{C_{lr} Q S b^2}{2 I_x u_0}$
$L_{\delta a} = \frac{C_{l\delta a} Q S b}{I_x}$	$N_{\beta} = u_0 N_v = \frac{C_{n\beta} QS}{I_z}$	$N_p = \frac{C_{np} Q S b^2}{2 I_z u_0}$
$N_r = \frac{C_{nr} Q S b^2}{2 I_z u_0}$	$Y_{\delta r} = \frac{C_{y\delta r} QS}{m}$	$N_{\delta a} = \frac{C_{n\delta a} Q S b}{I_z}$
$N_{\delta r} = \frac{C_{n\delta r} Q S b}{I_z}$	$L_{\delta r} = \frac{C_{l\delta r} Q S b}{I_x}$	-

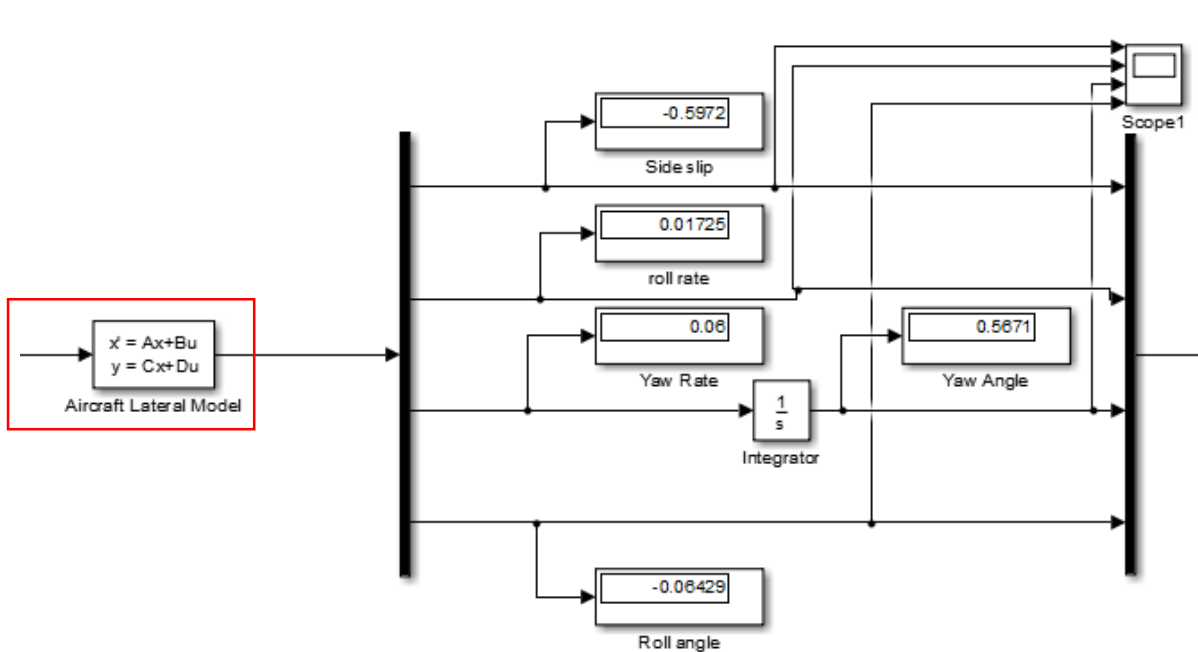


Figure 13 - Lateral Sub-System Model

The model generated in Simulink is shown in figure 13, it is just the lateral model of the flight dynamic system. The lateral matrix is contained within the block surrounded by the red box. Also the Simulink model uses the default values of $m_{\dot{\alpha}}$ produces a damping pole of 6.75×10^{-1} and 2.6×10^{-1} . However from analysis of the test flight cards, these values were considered to be unrealistic. As a result, the simulated value of $m_{\dot{\alpha}}$ is multiplied by a factor to damp and stabilise the system as suggested in '*Flight Stability and Automatic Control*'.^[4]

Figure 14 shows the graphical results of the both models working together, this allows to see whether the model is working as expected. The response that is modelled, couples phugoid, Dutch roll, and spiral together.

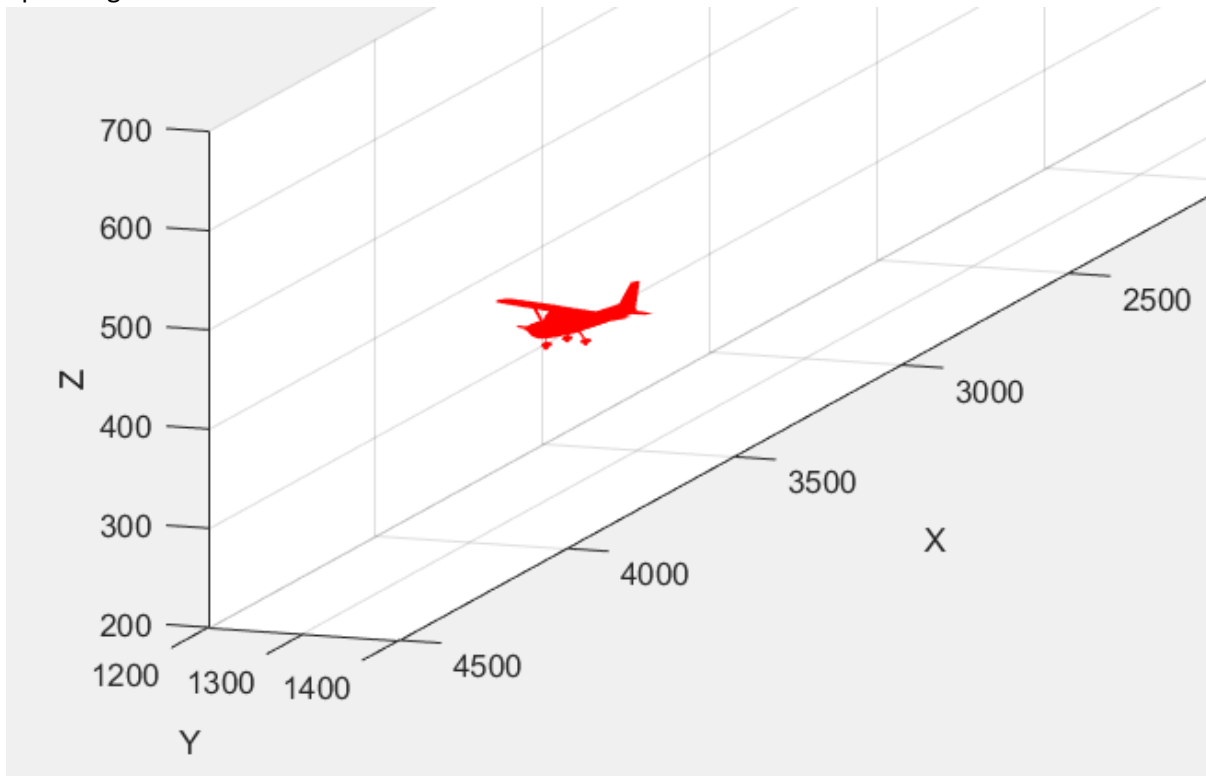


Figure 14 - Graphical Representation of Lateral Model

For yaw motion the damping ratio and undamped natural frequency needs to be found for the model, these variables can be determined from equations (5.15) and (5.16).

$$\omega_n = \sqrt{N_\beta} \quad (5.15)$$

$$\zeta = -\frac{N_r}{2\sqrt{N_\beta}} \quad (5.16)$$

5.6.1 Spiral Approximation

Spiral motion is when the aircraft enters a gradual spiralling motion. It is a non-oscillatory divergent motion that occurs when the directional stability is high and lateral stability is low, if no corrective action is taken then a high speed spiral dive is the result. Figure 15^[4] show the motion that is predicted.

Equations (5.17) is the characteristic root approximation. Both dihedral effect (L_β) and yaw rate damping (N_r) are usually negative while directional stability (N_β) and roll moment due to yaw rate (L_r) are normally positive. The increase the dihedral effect or yaw damping, can increase the spiral mode stability. ^[4]

$$\lambda_{spiral} = \frac{L_\beta N_r - L_r N_\beta}{L_\beta} \quad (5.17)$$

5.6.2 Roll Approximation

This motion can be approximated by equation (5.18). It is dependent on either the time constant of roll or the roll damping (L_p). The magnitude of L_p is dependent on the size of both the wing and tail surface areas. ^[4]

$$\lambda_{roll} = -\frac{1}{\tau} = L_p \quad (5.18)$$

5.6.3 Short Period Approximation

It is possible to approximate the damping ratios and frequency using the following equations (5.19) and (5.20). These are useful equations as have been proved to quite accurate, with a max percentage error of 3.03%. ^[13]

$$\omega_{sp} = \sqrt{\frac{Z_\alpha M_q - M_\alpha U_1}{U_1}} \quad (5.19)$$

$$2\zeta_{sp}\omega_{sp} = -\left(M_q + M_\alpha + \frac{Z_\alpha}{U_1}\right) \quad (5.20)$$

5.6.4 Dutch Roll Approximation

As the Dutch roll mode consists of mainly sideslipping and yawing and ignoring the rolling moment, equation (5.21) can be used. From here both the undamped natural frequency and damping can be found using equations (5.22) and (5.23) respectively. ^[4]

$$\begin{bmatrix} \Delta\dot{\beta} \\ \Delta\dot{r} \end{bmatrix} = \begin{bmatrix} \frac{Y_\beta}{u_0} & -\left(1 - \frac{Y_r}{u_0}\right) \\ N_\beta & N_r \end{bmatrix} \begin{bmatrix} \Delta\beta \\ \Delta r \end{bmatrix} \quad (5.21)$$

$$\omega_{n_{DR}} = \sqrt{\frac{Y_\beta N_r - N_\beta Y_r + u_0 N_\beta}{u_0}} \quad (5.22)$$

$$\zeta_{DR} = -\frac{1}{\omega_{n_{DR}}} \left(\frac{Y_\beta + u_0 N_r}{u_0} \right) \quad (5.23)$$

5.6.5 Phugoid Approximations

Section 4.5 approximates the phugoid motion in two degrees of freedom, however this is not perfect but it is better than Lanchester's approximations shown in equation (5.24). ^[13]

$$\omega_p = \frac{g\sqrt{2}}{U_1}$$

The approximation can be improved further by adding another degree of freedom to obtain improved values for frequency and damping ratio (equations (5.24) and (5.25)).

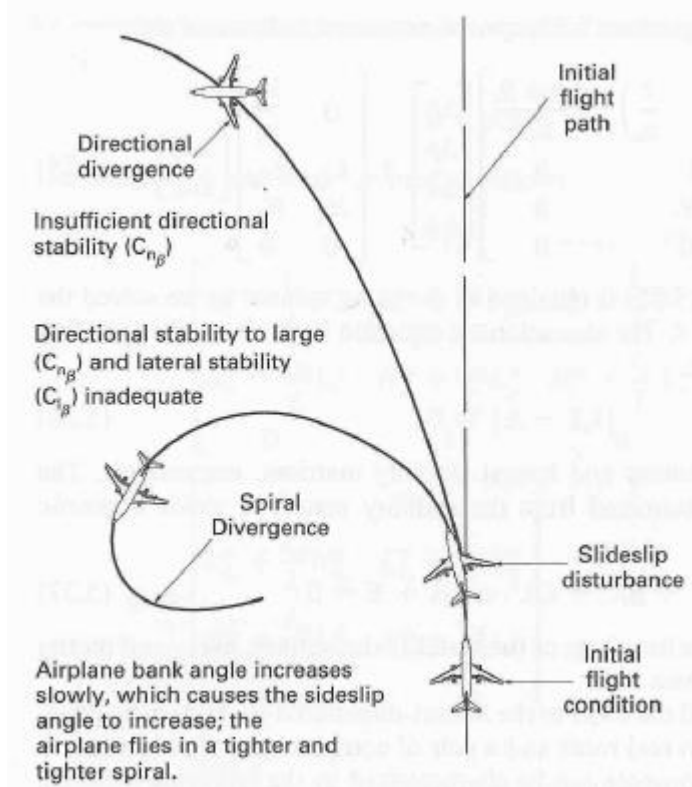


Figure 15 - Spiral Divergence

$$\omega_p = \sqrt{\frac{g(M_u Z_\alpha - Z_u M_\alpha)}{M_\alpha U_1}} \quad (5.24)$$

$$2\zeta_p \omega_p = -X_u + \frac{M_u(X_u - g)}{M_\alpha} \quad (5.25)$$

There are two other approximations that can be used to obtain phugoid motion frequencies and damping ratios. First is '*Bairstow's approximation*', which is based on knowledge of modal and fourth order characteristic equations. Through simplification the frequency and damping ratio can be seen in equations (5.26) and (5.27).^[13]

$$\omega_p = \sqrt{\frac{g(M_\alpha Z_u - M_u Z_\alpha)}{M_q Z_\alpha - U_1 M_\alpha}} \quad (5.25)$$

$$\zeta_p = \frac{-X_u}{2\omega_p} - \frac{\zeta_{sp} \omega_p}{\omega_{sp}} - \frac{M_u(U_1 X_w - g)}{2\omega_p \omega_{sp}^2} \quad (5.26)$$

However equation (5.26) can be expanded and simplified in terms of aerodynamics derivatives to:

$$2\zeta_p \omega_p = \frac{1}{M_\alpha U_1 - M_q Z_\alpha} \left(X_u (-M_\alpha U_1 + M_q Z_\alpha) + Z_u \left[-M_q X_\alpha + \frac{g M_\alpha (U_1 (M_\alpha + M_q) + Z_\alpha)}{M_\alpha U_1 - M_q Z_\alpha} \right] + M_u \left[U_1 X_\alpha - \frac{g (Z_\alpha (U_1 M_\alpha + Z_\alpha) + M_\alpha U_1^2)}{M_\alpha U_1 - M_q Z_\alpha} \right] \right) \quad (5.27)$$

The second method is '*Russell's approximation*', where the vertical and pitching accelerations are neglected as they are considered small in phugoid mode. The frequency and damping ratio are approximated by (5.28) and (5.29).

$$\omega_p = \sqrt{\frac{g M_\alpha Z_u}{M_q Z_\alpha - M_\alpha U_1}} \quad (5.28)$$

$$2\zeta_p \omega_p = -X_u + \frac{Z_u X_\alpha M_q}{M_\alpha U_1 - M_q Z_\alpha} \quad (5.29)$$

6.0 Results and System Model

6.1 Flight Dynamic Model

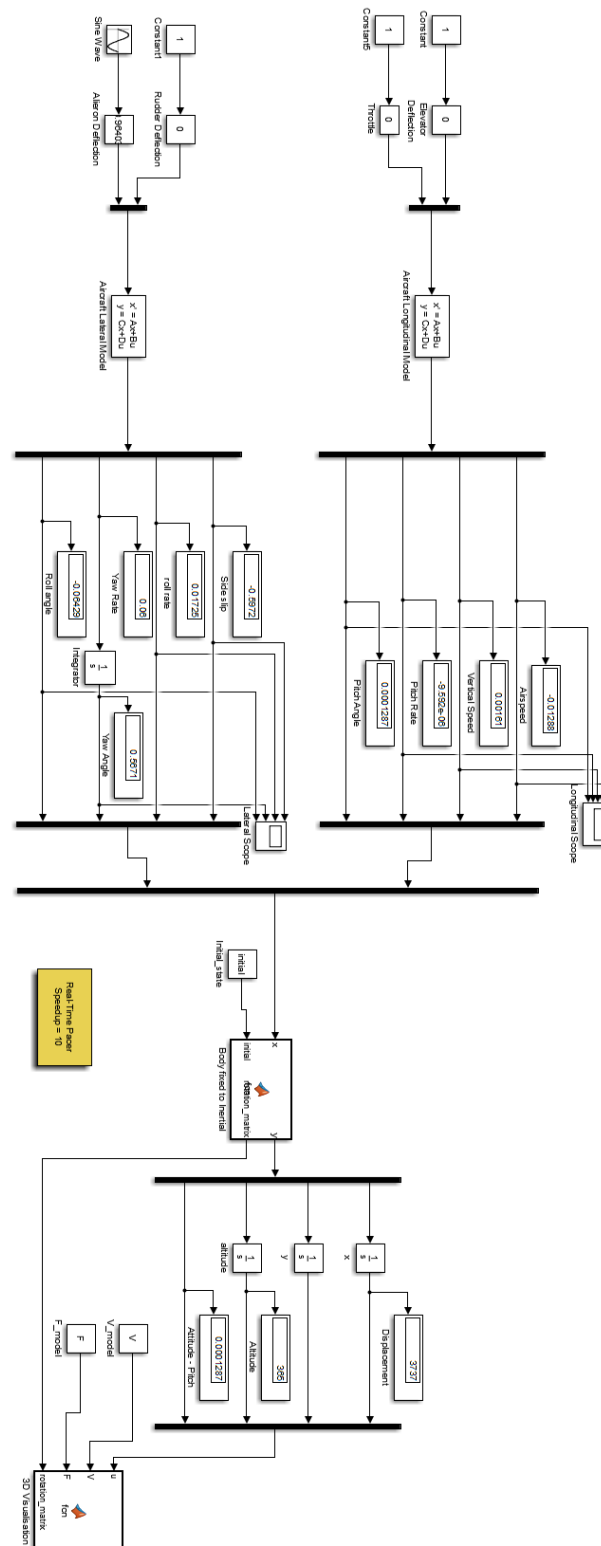


Figure 16 - Flight Dynamic System

6.2 Results

6.3.1 Phugoid, Short Period and Dutch Roll

Table 9 shows the response variables, natural frequency and damping ratio, from both the data sets and the theoretical approximations. The values from the flight data, MATLAB and Bairstow's approximation return similar phugoid damping ratio values, while those values from 2, 3 degrees of freedom and Russell's approximation are similar. However for the natural frequency the values remain similar only for the approximation's, except Lanchester's.

The variance that is observed could be from a different factors. Firstly the flight data that is recorded may not be accurate, due to human errors, lack of data or instrumentation failures. Secondly the flight dynamic model made in Simulink may be incorrect due to the flight data that is inaccurate, as the phugoid motion to be modelled is taken from the flight test data. Also the model may have errors within the script, resulting with an error being multiplied through various equations resulting in a greater deviation from the correct answer. Lastly the model may just be incorrect in one or more axes resulting in the difference.

Lanchester's approximation returns a value that is too high, and would be deemed to be inaccurate as the model implies that only phugoid frequency only depends on the forward velocity.

Regarding Dutch roll the variables between the flight data and that generated by MATLAB differ quite, with the flight the data stating that the motion is underdamped whereas the MALAB script states that the aircraft is overdamped. Both models do suggest that the EV-97 has stability in a Dutch roll.

The short period approximation looks correct as after finding the period of the mode, using equation (6.0) ^[9], it falls within predictable ranges for microlights.

$$T_{sp} = \frac{2\pi}{\omega_{nsp}\sqrt{1-\zeta_{sp}^2}} = 6.04 \text{ s (6.0)}$$

Table 9 - Damping Ratio and Natural Frequency Table

	Variable	Phugoid	Short Period	Dutch Roll
Flight Data	Damping Ratio (ζ)	0.300291	-	0.620065
	Natural Frequency (ω_n)	0.7866	-	0.866729
MATLAB/Simulink	Damping Ratio (ζ)	0.2966	-	0.00579
	Natural Frequency (ω_n)	0.2632	-	2.4651
Short Period Approximation	Damping Ratio (ζ)	-	0.849765	-
	Natural Frequency (ω_n)	-	1.971829	-
Lanchester Approximation	Damping Ratio (ζ)	-	-	-
	Natural Frequency (ω_n)	7.381057	-	-
2 Degrees of Freedom	Damping Ratio (ζ)	-0.068523	-	-
	Natural Frequency (ω_n)	1.147065	-	-
3 Degrees of Freedom	Damping Ratio (ζ)	-0.068522	-	-
	Natural Frequency (ω_n)	1.147065	-	-
Bairstow's Approximation	Damping Ratio (ζ)	0.397878	-	-
	Natural Frequency (ω_n)	1.023244	-	-
Russell's Approximation	Damping Ratio (ζ)	0.076107	-	-
	Natural Frequency (ω_n)	1.025408	-	-

6.2.2 Simulink Model

From the Simulink model shown in figure 16, numerous graphs can be obtained from it. Figures 17 and 18 show the scope and responses obtained from the system, over a time period of 120 seconds. The longitudinal matrix shows predictable and damped responses. On the other hand the lateral matrix in figure 18, shows unexpected responses.

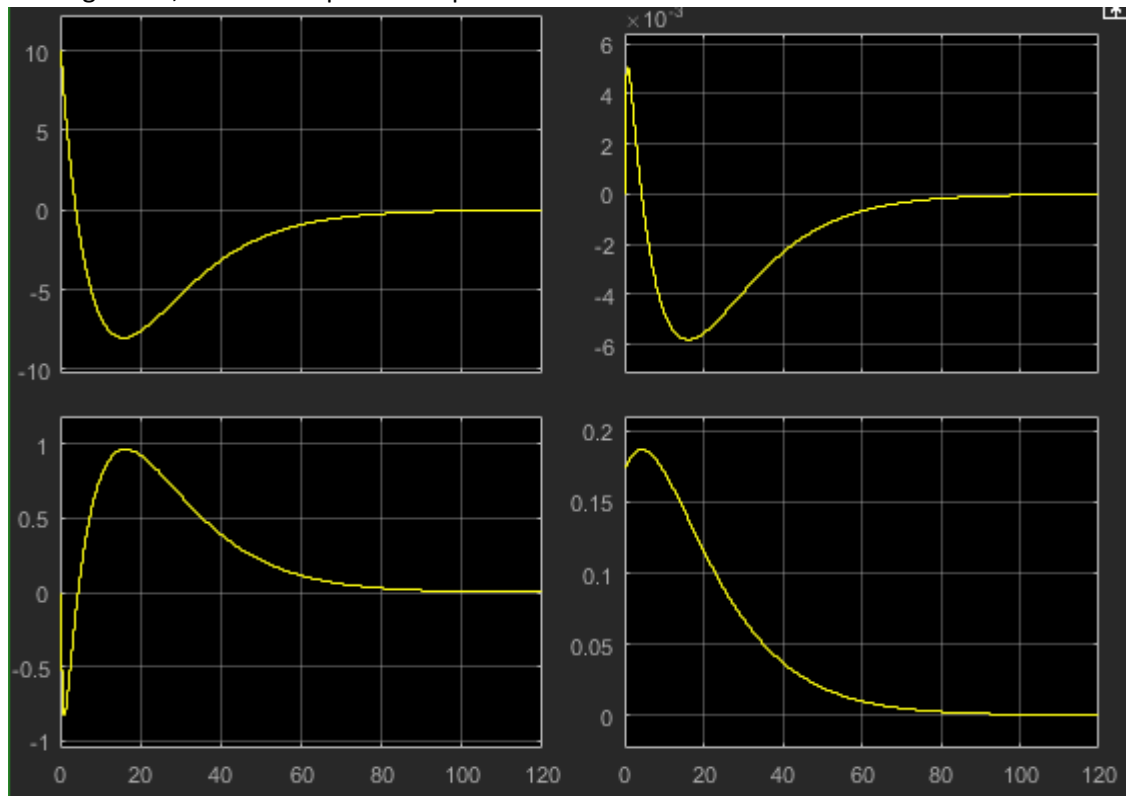


Figure 18 - Longitudinal Scope

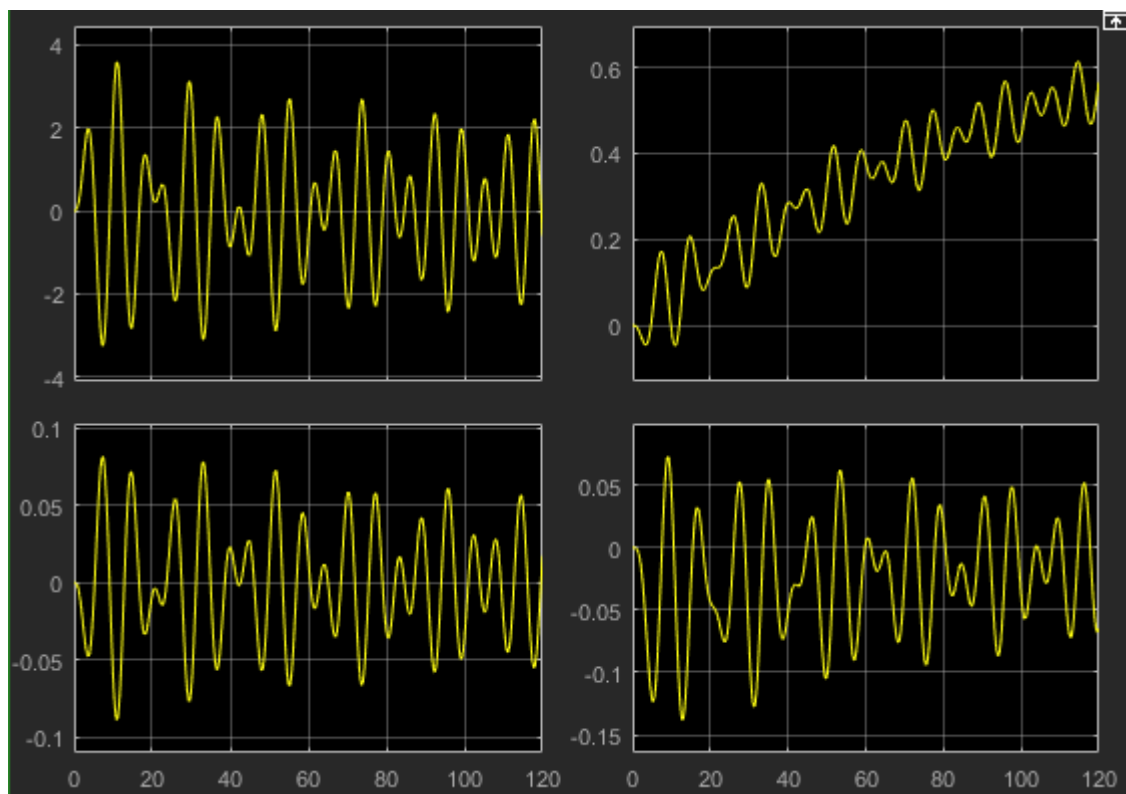


Figure 17 - Lateral Scope

Observing figure 19, we can see that the in the longitudinal matrix in both the vertical and horizontal airspeeds are critically damped which is expected. While the roll rate and angle response minimally responds, however it does produce the required reaction for the system to be stable in the Z axis.

- Vertical Speed – Blue
- Airspeed – Red
- Roll Rate – Orange
- Roll Angle – Pink

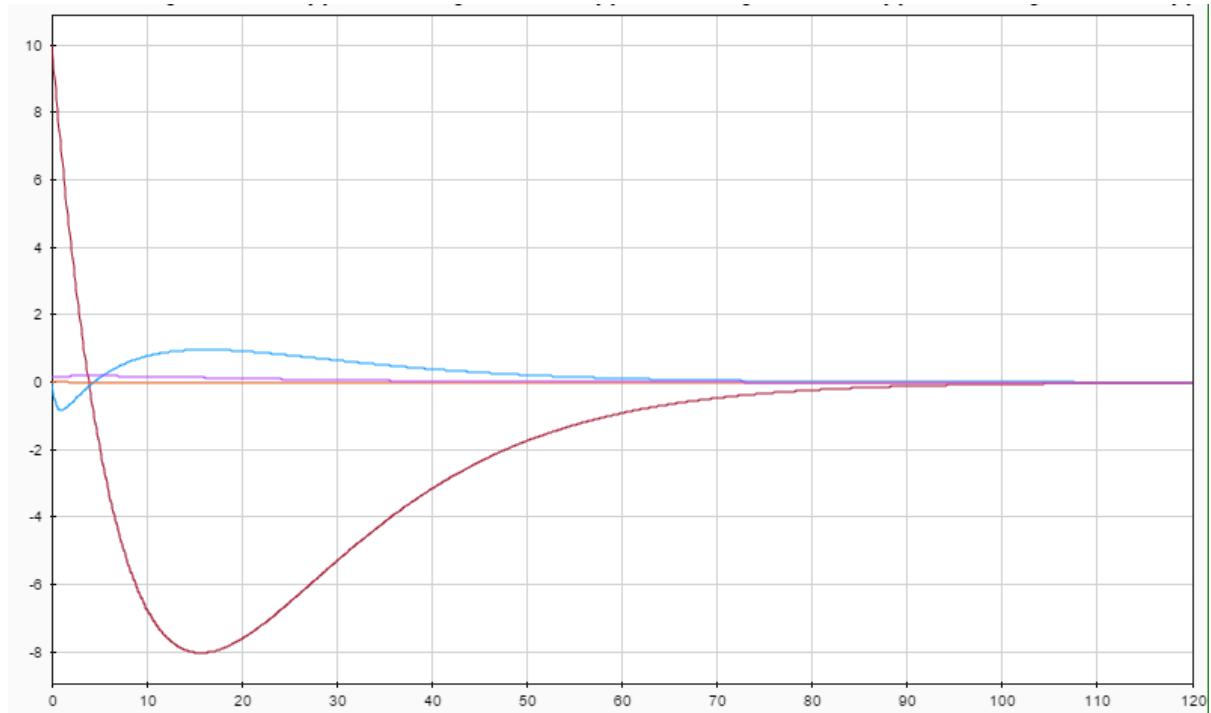


Figure 19 - Longitudinal Matrix Graph

Figure 20 shows the lateral simulation graph, combining the yaw rate, sideslip and angle alongside the roll rate.

- Yaw Sideslip – Red
- Roll Rate – Yellow
- Yaw Rate – Purple
- Yaw Angle - Green

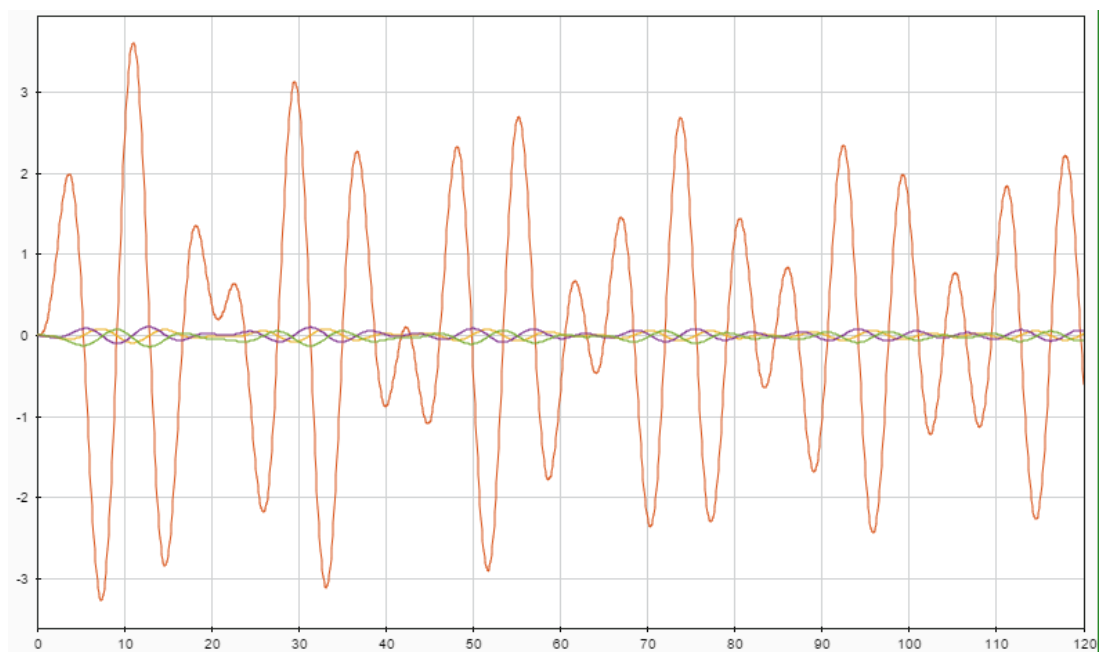


Figure 20 -Lateral Matrix Graph

From the lateral model the yaw rate, angle and roll rate remain almost constant with a slight decrease in amplitude, which suggests that they have a damping ratio of almost zero. This motion isn't particularly noticeable in the 3D visualisation and would be expected when flying in atmospheric conditions. However the yaw sideslip oscillates without any damping which was an unexpected result, this shows that is isn't damped in the motion and it is represented in the visualisation, as shown from figures 21 and 22.

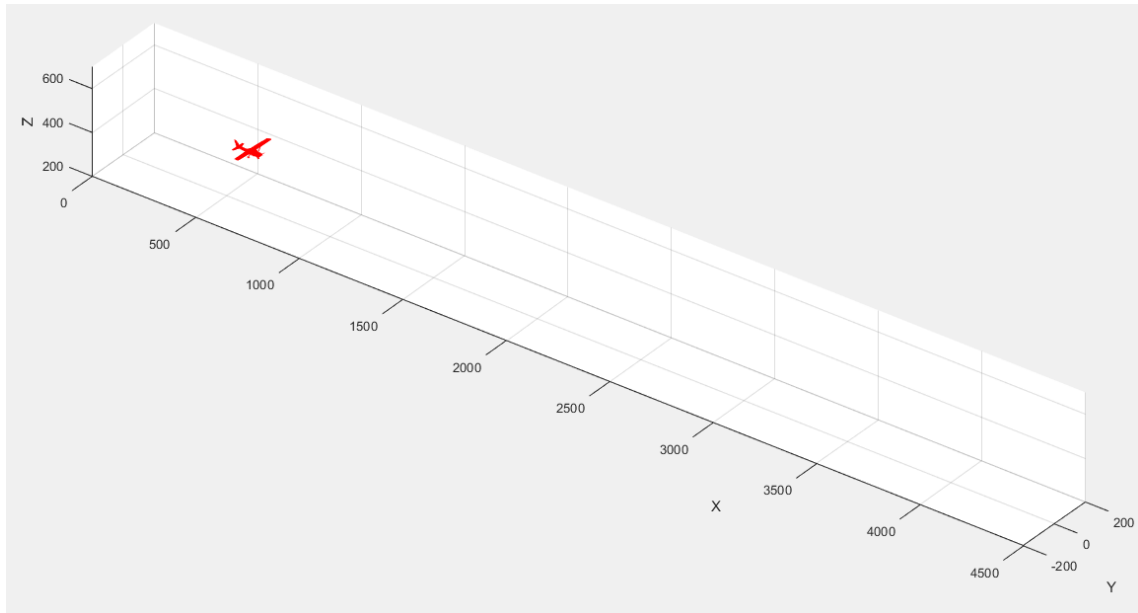


Figure 22 – Beginning of 3D Visualisation

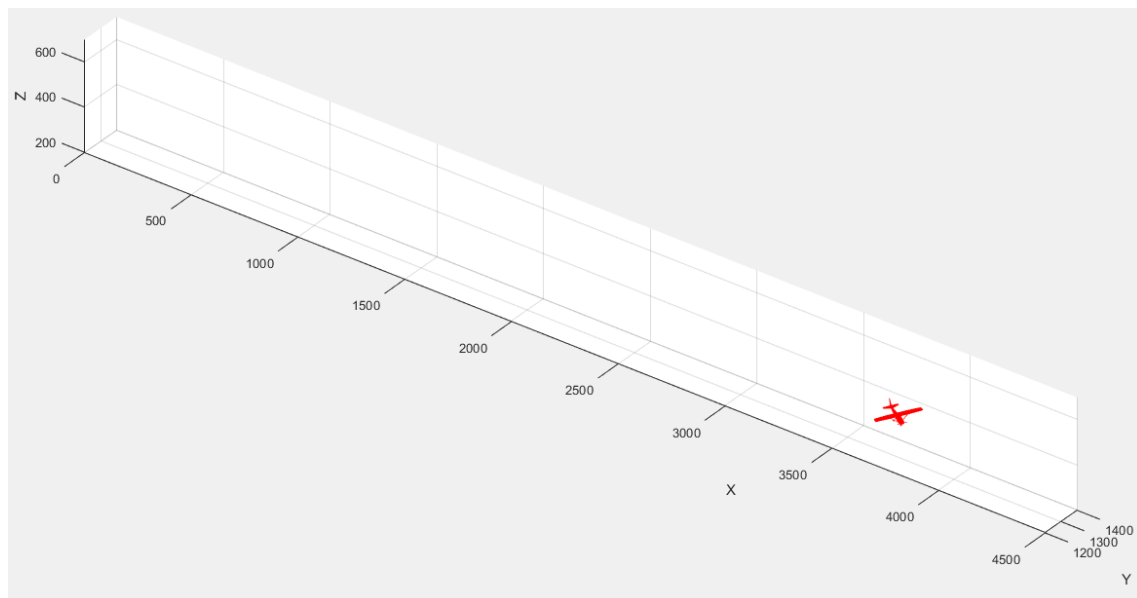


Figure 21 - End positon in 3D Visualisation

This sideslip that is observed is undesirable as it shows the instability of the lateral flight model without it able to maintain a constant heading. The lateral model must have an error contained within the script, most likely related with the yaw angle. On the other hand this divergence was observed in the actual flight testing, as shown in figure 23. This would be due to the low weight of the aircraft and the possibility of the weight not being balanced on the aircraft.

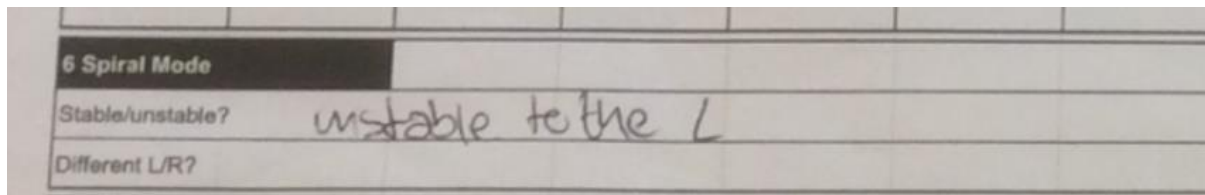


Figure 23 - Test Card with observed Spiral Instability

In actual flight, directional divergence would be countered by adjusting the trim on the aircraft so that the sideslip is accounted for. This could be modelled within the aircraft by adjusting the rudder angle so that the aircraft will remain on a constant heading.

6.3 Improvements

This section will discuss possible improvements to increase accuracy of model and results.

6.3.1 Flight Data Improvements

An initial improvement would be to collect more flight test data. An increased range of data would allow for better approximations of the different flight motions, reducing environmental effects and reduce the human errors made when recording the results. Another variable that should be recorded in future flight data, is the weather conditions during testing, as this will affect the results.

Also instead of manually record the data, the data could be collected from a computational data logger connecting to instrumentation. This would allow for more precise measurements and easier repeatability.

6.3.2 Model Improvements

To improve the model particular focus into solving the directional divergence that is observed in the model, as it is currently not understood why this is observed. An investigation to see why there is insufficient directional stability ($C_{n\beta}$) and how to solve it would need to be completed, and also why spiral divergence isn't observed from this instability.

Another improvement would be to add weather conditions and wind directions to the model, this would be to simulate their effects upon the aircraft and to see how they affect the stability and oscillatory response. Lastly a cosmetic change to the system by changing the Cessna aircraft model to a EV-97 model to be shown in MATLAB.

6.3.3 MERLIN Flight Simulator

To improve overall accuracy of the project, the MERLIN flight simulator could be used. This would allow for another data set to be obtained for comparison. It runs on a flight software called EXCALIBUR, which models aircraft six degrees of freedom and is a fully non-linear transonic application. It allows for almost any type of aircraft to be simulated, including prototypes. [13] Figure 24 shows the supplied flight model editor, this allows for almost all variables to be considered.

The EXCALIBUR Flight Model Editor interface includes the following sections:

- Aircraft Mass:** Empty Mass (1605 kg), Empty CG x (0.0 m), Empty CG y (0.0 m), Empty CG z (0.0 m).
- Fuel:** Fuel Capacity (400 kg), x Location (0.0 m), y Location (0.0 m), z Location (0.0 m).
- Pilot Eye Position:** x (1.5 m), y (1.0 m), z (-0.5 m).
- Aircraft Empty Inertia:** Ixx (5445 kg.m²), Iyy (2235 kg.m²), Izz (7834 kg.m²), Ixz (783 kg.m²), Wing Span (11.0 m).
- Payloads:** A table with 5 columns for different payload configurations, including Initial/Final Mass, Initial/Final x/y/z, Deploy Time, and Reload Time.
- Aircraft Axes:** X (positive FORWARD), Y (positive RIGHT), Z (positive DOWN).
- Warning:** Do Not Leave Any Boxes Blank!

Figure 24 - EXCALIBUR Flight Model Editor

7.0 Conclusion

In conclusion, the aim of the investigation was partially met as data from the real world was successfully compared and contrasted to the Simulink model, including information regarding a number of stability components. As was expected, there is some variance between the recorded experimental data and the calculated simulated data. This is due to a number of factors including but not limited to human error, instrument failure and inaccuracies in the modelling. The longitudinal model created acted as expected however when modelling the lateral model, complications arose that meant the model did not behave as was expected. The yaw motion represented in the model is effectively undamped and therefore unrealistic. With more time, the model could be improved upon, but as it stands, the lateral data outputted is of little use. The problem undoubtedly lies in the code for the model and should be looked over to find the cause of the problem. To test even further, the model could be used in a flight simulator to corroborate any and all data produced.

8.0 References

- [1] - Cutler, C (2015). *The 3 Types Of Static And Dynamic Aircraft Stability*. Available from: <http://www.boldmethod.com/learn-to-fly/aerodynamics/3-types-of-static-and-dynamic-stability-in-aircraft/> [Accessed: 2/11/2015]
- [2] - Evektor-Aerotechnik (2004). *EV-97 teamEUROSTAR UK Pilot's Operating Handbook*. Available from: www.blackboard.uwe.ac.uk/ [Accessed: 28/09/2015]-
- [3] - Evektor-Aerotechnik (2008). *AIRPLANE TECHNICAL DESCRIPTION OPERATING, MAINTENANCE AND REPAIR MANUAL EV-97 Eurostar SL* [Online]. Czech Republic: Evektor-Aerotechnik. (1). Available from: www.blackboard.uwe.ac.uk/ [Accessed: 28/09/2015]
- [4] - Nelson, R (1998). *Flight Stability and Automatic Control*. 2nd Ed. United States: McGraw-Hill.
- [5] - Flight Laboratory IIT Kanpur (2015). *Longitudinal & Lateral Airplane Dynamics*. Available from: <http://www.iitk.ac.in/aero/fltlab/dynamics.html>. [Accessed: 21/11/2015]
- [6] - Pritesh, N (2015). 'Week 12: Flight Mode Approximation and Analysis'. UFMFCH-15-3 Spaceflight. Available from: <https://blackboard.uwe.ac.uk> [Accessed: 20/10/2015]
- [7] - The Logbook (2012). *Aerodynamics/Principles of Flight*. Available from: <http://herschlogbook.blogspot.co.uk/2012/07/aerodynamics-principles-of-flight.html> [Accessed: 21/11/2015]
- [8] - Rochester Institute of Technology (2015). *Roots: Lateral – Directional Motion*. Available from: http://people.rit.edu/pnveme/EMEM682n/DynamicStab/roots_lateral.html [Accessed: 21/11/2015]
- [9] - Cornell University (2015). *Chapter 5 Dynamic Stability*. Available from: <https://courses.cit.cornell.edu/mae5070/DynamicStability.pdf> [Accessed: 21/11/2015]
- [10] - Brits, L (2008). *Proper Euler angles representing rotations about X, Y, and Z axes* [Image] At: Wikipedia [Online] Available from: https://en.wikipedia.org/wiki/Euler_angles#/media/File:Eulerangles.svg [Accessed: 22/11/2015]
- [11] - Pritesh, N (2015). 'Week 11: Navigation via Euler Angles and Quaternions'. UFMFCH-15-3 Spaceflight. Available from: <https://blackboard.uwe.ac.uk/> [Accessed: 21/11/2015]
- [12] - Pritesh, N (2015). 'Week10: Rigid Body Aircraft Equations of Motion'. UFMFCH-15-3 Spaceflight. Available from: <https://blackboard.uwe.ac.uk/> [Accessed: 21/11/2015]
- [13] - Pradeep, S (1998). A Century of Phugoid Approximations. *Aircraft Design*. [Online]. 1, pp. 89-104. [Accessed: 2/11/2015]
- [14] - Merlin Flight Simulation Group (2009). *MERLIN Flight Simulation Group Excellence in Motion*. Available from: <http://www.merlinsim.com/index.htm> [Accessed: 25/11/2015]

9.0 Appendix

9.1 Flight Test Card A



University Experimental Flight Mechanics

Team		Flight Profile		A	
Aircraft				Date	
Met	QNH	mb	Temp		deg C
Crew L			Wgt	lbs	
Crew R			Wgt	lbs	
Rear L			Wgt	lbs	
Rear R			Wgt	lbs	
Fuel	Take Off	US gal	Landing	US gal	
Timings					
Tacho Start	Brakes Off	Take Off	Landing	Brakes On	Tacho Finish
GMT / BST					
1 Climb Performance			Speed	Start Height	End Height
2 Phugoid					
Period:		seconds for	cycles		
Damping:					
3 Roll Mode					
Time to subside?					
Different L/R?					
4 Roll Control Task			HQR		
5 Spiral Mode					
Stable/unstable?					
Different L/R?					
6 Long Static Stab					
7 Descent Performance			Speed	Start Height	End Height

9.2 Flight test Card B



University Experimental Flight Mechanics

Team		Flight Profile		B	
Aircraft			Date		
Met	QNH	mb	Temp	deg C	
Crew L			Wgt	lbs	
Crew R			Wgt	lbs	
Rear L			Wgt	lbs	
Rear R			Wgt	lbs	
Fuel	Take Off	US gal	Landing	US gal	
Timings					
Tacho Start	Brakes Off	Take Off	Landing	Brakes On	Tacho Finish
		GMT / BST			
1 Climb Performance		Speed	Start Height	End Height	Time
2 Short Period Mode					
Damping?					
Period?					
3 Height Control Task				HQR	
4 Dutch Roll Mode					
Damping?					
Period?					
5 Heading Control Task				HQR	
6 Steady Heading Sideslip					
7 Descent Performance		Speed	Start Height	End Height	Time